Wrinkling Instability in Unsupported Epithelial Sheets

Urška Andrenšek,[1,2] Primož Ziherl,[1,2] and Matej Krajnc[2,*]
[1]Faculty of Mathematics and Physics, University of Ljubljana, Jadranska 19, SI-1000 Ljubljana, Slovenia
[2]Jožef Stefan Institute, Jamova 39, SI-1000 Ljubljana, Slovenia

(Received 21 October 2022; accepted 20 April 2023; published 11 May 2023)

We investigate the elasticity of an unsupported epithelial monolayer and we discover that unlike a thin solid plate, which wrinkles if geometrically incompatible with the underlying substrate, the epithelium may do so even in the absence of the substrate. From a cell-based model, we derive an exact elasticity theory and discover wrinkling driven by the differential apico-basal surface tension. Our theory is mapped onto that for supported plates by introducing a phantom substrate whose stiffness is finite beyond a critical differential tension. This suggests a new mechanism for an autonomous control of tissues over the length scale of their surface patterns.

DOI: 10.1103/PhysRevLett.130.198401

Introduction.—Complex shapes and patterns often arise even in simple physical setups [1–3]. For instance, a uniaxial in-plane compression makes a thin plate attached to an elastic foundation wrinkle due to the competition between the bending energy of the plate and the bulk elastic energy of the substrate [4,5]. This competition yields the length scale of wrinkles, which scales with the ratio of the stiffness coefficient of the foundation K and the bending modulus of the plate B as [5–7]

$$\lambda_0 \sim \left(\frac{K}{B}\right)^{-1/3}. \tag{1}$$

In proliferating epithelia, cell division causes areal growth of the tissue relative to the underlying stroma. The proliferation-driven differential growth leads to a geometric incompatibility between the epithelium and the stroma, triggering wrinkling with the wavelength given by Eq. (1) much like an external compressive force [8,9].

Periodic surface patterns in epithelia may also arise from the intrinsic curvature due to apico-basal differential surface tension, which is known to drive characteristic local deformations such as epithelial curling and buckling *in vitro* [10–12] as well as folding during morphogenesis and organogenesis [13–15]. This mechanism may be particularly relevant in unsupported epithelia, whose deformations mostly rely on internal active stresses. We previously investigated such cases and we showed that the differential tension alone can produce periodic deformation patterns even if the tissue is not attached to a substrate [16–18]. However, these studies only considered the large-deformation regime where the equilibrium wavelength is mainly determined by steric interactions between cells, and they neither identified the parameters that control the wavelength of shape patterns at the onset of wrinkling nor did they show why epithelia wrinkle in the absence of the substrate in the first place.

Here, we address these issues by deriving an elasticity theory from the cell-level mechanics based on surface tension. Our theory describes a new type of tension-controlled transition whereby tissues switch between the buckling instability, where they buckle out of plane, and the wrinkling instability, where their deformation pattern is characterized by a finite wavelength. We show that the effect of surface tensions can be translated into the stiffness of a phantom bulk substrate, which becomes finite at the critical point. This concept reconciles the wrinkling of unsupported epithelia with that of thin solid plates supported by substrates, and it serves as a basis of a novel mechanism for autonomous control of shape patterns in epithelia.

The model.—Our model tissue is represented by a chain of quadrilateral cell cross sections [Fig. 1(a)]. The basal, apical, and lateral cell sides are under effective line tensions Γ_b, Γ_a, and Γ_l, respectively, which account for cortical tension, apico-basal differential surface tension, describing apico-basal tension polarity, and cell-cell

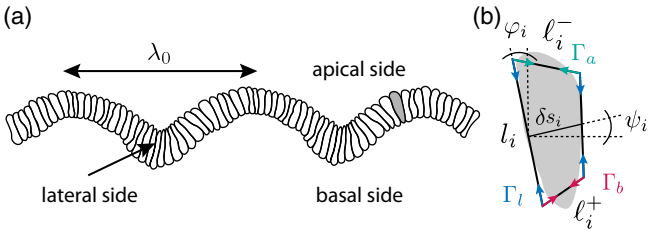

FIG. 1. (a) Waveform of a wrinkled epithelial monolayer, its wavelength denoted by λ_0. (b) Schematic of a cell cross section, parameterized by two lengths (l_i and δs_i) and two angles (φ_i and ψ_i). The line tensions of the basal, apical, and lateral sides read Γ_b, Γ_a, and Γ_l, respectively.

adhesion. Following previous models, we view all three terms as strain-independent and we model them by constant line tensions [16,18,19]. The cells are assumed incompressible, and therefore their cross-section areas are fixed and equal in all cells ($A_i = A_0$ for all i).

We parameterize the shape of ith cell by the lengths of its lateral sides l_i and l_{i+1}, cell width δs_i, the orientation of lateral sides relative to the vertical axis given by angles φ_i and φ_{i+1}, respectively, and the orientation of cell midline relative to the horizontal axis given by angle ψ_i [Fig. 1(b)]. The constant-cell-area constraint allows us to express δs_i in terms of all other variables, so that in dimensionless form, where energy and lengths are given in units of $\Gamma_l\sqrt{A_0}$ and $\sqrt{A_0}$, respectively, the energy of a single cell reads

$$w_i = \frac{\Gamma_b}{\Gamma_l}\ell_i^+ + \frac{\Gamma_a}{\Gamma_l}\ell_i^- + \frac{1}{2}(l_i + l_{i+1}), \tag{2}$$

where the lengths of basal and apical cell sides ℓ_i^+ and ℓ_i^-, respectively, depend on l_i, l_{i+1}, φ_i, φ_{i+1}, and ψ_i (Supplemental Material, Sec. I [20]). Next we define the average and the differential apico-basal surface tension

$$\Gamma = \frac{\Gamma_a + \Gamma_b}{\Gamma_l} \quad \text{and} \quad \Delta = \frac{\Gamma_a - \Gamma_b}{\Gamma_l}, \tag{3}$$

respectively, and we study homogeneous tissues where Γ is the same in all cells and so is Δ. The energy of the tissue is a sum of single-cell terms: $W = \sum_i^N w_i$.

Epithelial elasticity.—Unlike the classical plate theory that stems from the strain distribution within the plate, the elasticity of our model tissue arises from surface mechanics. Interestingly, this affects the scaling of the stretching and bending moduli (K_s and B, respectively) with tissue thickness l_0. Considering only pure stretching and bending deformation modes, we find that $K_s \sim l_0^2$ and $B \sim 1$, which differs from the well-known results for solid plates where $K_s^{\text{plate}} \sim l_0$ and $B^{\text{plate}} \sim l_0^3$ (Supplemental Material, Sec. II [20]). Since wrinkles result from the competition between the two deformation modes, this scaling suggests that epithelial wrinkling is phenomenologically distinct from that in plates.

To derive the exact elastic theory, we consider a deformation from the flat reference state where $l_i = l_0 = \sigma_0^{-1}$, $\varphi_i = 0$, and $\psi_i = 0$; here, $\sigma_0 = \Gamma^{-1/2}$ is the reference cell width. We view l_i, δs_i, φ_i, and ψ_i as continuous functions of the distance σ along the reference-state midline so that $l_i \to l(\sigma)$, etc., and we relate their values in the $(i+1)$th and ith cell by their derivatives with respect to σ: $l_{i+1} \approx l(\sigma) + \dot{l}(\sigma)\sigma_0$, etc. In the continuum limit, the sum over cells is replaced by the integral over the reference-state midline and the energy reads $W = \int_0^{N\sigma_0} \mathcal{L} d\sigma = \Gamma^{1/2}\int_0^{N\sigma_0}[w(l,\varphi,\psi,\dot{l},\dot{\varphi}) + \mu\delta s(l,\varphi,\psi,\dot{l},\dot{\varphi})\cos\psi]d\sigma$. Here, the Lagrange multiplier μ represents the compressive force.

We expand the Lagrangian density $\mathcal{L}$ for small deviations from the reference state up to the second order and we obtain

$$\begin{aligned}\mathcal{L} \approx{}& 2\Gamma + \mu - \frac{\mu}{\sqrt{\Gamma}}\delta l - \frac{\Delta\sqrt{\Gamma}}{2}\dot{\varphi} + \frac{\Gamma-\mu}{2}(\psi-\varphi)^2 \\ &+ \frac{\mu}{2}\psi^2 + \frac{\Gamma+\mu}{\Gamma}\delta l^2 + \delta l\left(\frac{1}{\sqrt{\Gamma}}\delta\dot{l} - \frac{\Delta}{2}\dot{\varphi}\right) \\ &+ (\psi-\varphi)\left(\frac{\Delta}{2}\delta\dot{l} - \frac{\sqrt{\Gamma}}{2}\dot{\varphi}\right) - \frac{\mu}{2\sqrt{\Gamma}}\psi\dot{\varphi} \\ &- \frac{\Delta}{2\sqrt{\Gamma}}\delta\dot{l}\,\dot{\varphi} + \frac{2(\mu+\Gamma)+\Gamma^3}{8\Gamma^2}\delta\dot{l}^2 + \frac{\mu+\Gamma}{4\Gamma}\dot{\varphi}^2,\end{aligned} \tag{4}$$

where $\delta l = l - l_0$ is the deviation of the lateral-side length from the reference value. Next we spell out the Euler-Lagrange equations (Supplemental Material, Sec. III [20]) and Fourier transform $\delta l(\sigma)$, $\varphi(\sigma)$, and $\psi(\sigma)$: $\delta l(\sigma) = \int \delta\tilde{l}(q)\exp(iq\sigma)dq/2\pi$, etc. where $q = 2\pi/\lambda$. These transformations reduce the Euler-Lagrange equations to a single algebraic equation for the wave number of the instability:

$$q_0^4 + \tilde{F}q_0^2 + \tilde{K} = 0, \tag{5}$$

where $\tilde{F}$ and $\tilde{K}$ are functions of Γ, Δ, and μ (Supplemental Material, Sec. IV [20]). Surprisingly, even though our epithelial sheets are neither thin (as their thickness is generally not negligible compared to the wrinkle wavelength) nor supported by a substrate, Eq. (5) is equivalent to the version of Eq. (7) in Ref. [7] that describes wrinkling of thin plates on a liquid foundation [21]. By this analogy, $\tilde{F}$ and $\tilde{K}$ can be viewed as an effective in-plane force and an effective stiffness of a "phantom" substrate, respectively, both expressed relative to the bending modulus of the epithelium.

Our system becomes unstable at a critical in-plane compressive force $\mu = \mu_c$ (Supplemental Material, Sec. IV [20]), with the mode of instability switching from buckling to wrinkling as the magnitude of the differential surface tension $|\Delta|$ is increased beyond $\Delta_c = \sqrt{2}$. This transition is nicely reflected in the critical values of the two effective parameters $\tilde{F}_c$ and $\tilde{K}_c$ corresponding to μ_c. In particular, for $|\Delta| < \Delta_c$ the critical in-plane force $\tilde{F}_c > 0$, whereas the critical substrate stiffness $\tilde{K}_c = 0$ so that the phantom substrate is absent [Fig. 2(a)]. In this regime, Eq. (5) simplifies to $q_0^2(q_0^2 + \tilde{F}_c) = 0$ and its only real solution $q_0 = 0$ implies buckling under compression [Fig. 2(b)] as expected for unsupported plates.

However, at $|\Delta| > \Delta_c$, $\tilde{F}_c$ is negative (indicating a contractile tissue), whereas $\tilde{K}_c$ is positive, which signals the presence of a phantom substrate [Fig. 2(a)]. In this regime, Eq. (5) has a double real solution at a critical in-plane compressive force μ_c [Fig. 2(b)], implying

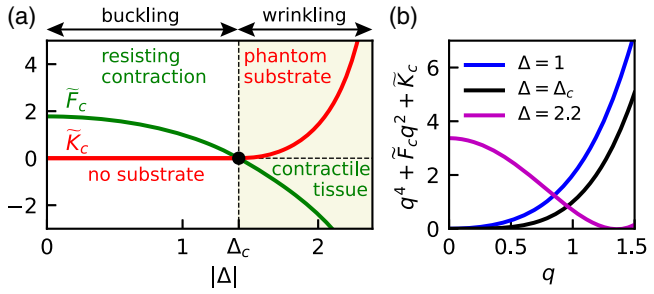

FIG. 2. (a) $\tilde{F}_c(\Delta)$ (green curve) and $\tilde{K}_c(\Delta)$ (red curve). (b) Left-hand side of Eq. (5) for $\Delta = 1$, $\Delta_c(=\sqrt{2})$, and 2.2 (blue, black, and purple curves, respectively). In both panels, $\Gamma = 4$.

$\tilde{F}_c = -2\tilde{K}_c^{1/2}$. Thus, Eq. (5) reduces to $(q_0^2 - \tilde{K}_c^{1/2})^2 = 0$ and its solution $q_0 = \tilde{K}_c^{1/4}$ describes wrinkles with a wavelength

$$\lambda_0 = 2\pi\tilde{K}_c^{-1/4}. \tag{6}$$

This result agrees with that for thin elastic plates supported by a thick *liquid* foundation [7]. Importantly, the scaling exponent in Eq. (6) differs from $-1/3$ obtained in the case where the epithelium is treated as a thin plate attached to a thick elastic substrate [Eq. (1) and Ref. [8]].

Interestingly, the critical external in-plane force μ_c also changes sign at $|\Delta| = \sqrt{2}$, such that an extensile force is required in the wrinkling regime so as to prevent tissue collapse. If a collapse *is* allowed, the equilibrium wavelength is determined by steric repulsion and is of the order of twice the cell height ($\lambda_0 \sim 2\sigma_0^{-1}$) and almost independent of Δ [16].

Vertex model.—To address cell-level mechanisms of the buckling-to-wrinkling transition, we next employ the vertex model where the tissue shape is parameterized by the positions of cell vertices. The equilibrium wrinkled and buckled states are computed by minimizing the total energy $W = \sum_i^N w_i$ and the size of the simulation box is varied so as to find the critical compressive force at which the instability occurs [Figs. 3(a) and 3(b) and Supplemental Material, Sec. V [20]].

We compute the equilibrium wavelength λ_0 for a wide range of parameters Γ and Δ. By interpreting $q_0 = 2\pi/\lambda_0$ and $|\Delta|$ as an order and a control parameter, respectively, we find a second-order buckling-to-wrinkling transition at $|\Delta| = \Delta_c = \sqrt{2}$. We compare the results to the elastic theory by plotting the wave number of wrinkles q_0 versus the control parameter $|\Delta|$ and in the regime where the wavelengths are much longer than the typical cell size and the continuum approximation is justified, we find perfect agreement [Fig. 3(c)]. The data also agree with the critical scaling of the wave number

$$q_0 \approx \frac{2^{5/4}}{\sqrt{\Gamma - 2/\Gamma}}(|\Delta| - \Delta_c)^{1/2} \tag{7}$$

obtained by studying our theory around $|\Delta| = \sqrt{2}$. Furthermore, the data can be collapsed onto a universal curve given by Eq. (6) by plotting the equilibrium wavelength versus the critical substrate stiffness $\tilde{K}_c$ given by Eq. (S34) [Fig. 3(d)]. This confirms that in the context of wrinkling, the surface tensions of the cells give rise to mechanics that are indistinguishable from the bulk elasticity of thick substrates.

Cell-height modulation.—The origin of the wrinkling instability can be intuitively understood by inspecting the shape of individual cells along the waveform. This shows that cell height is modulated in agreement with the elastic theory, which predicts that the modulation is proportional

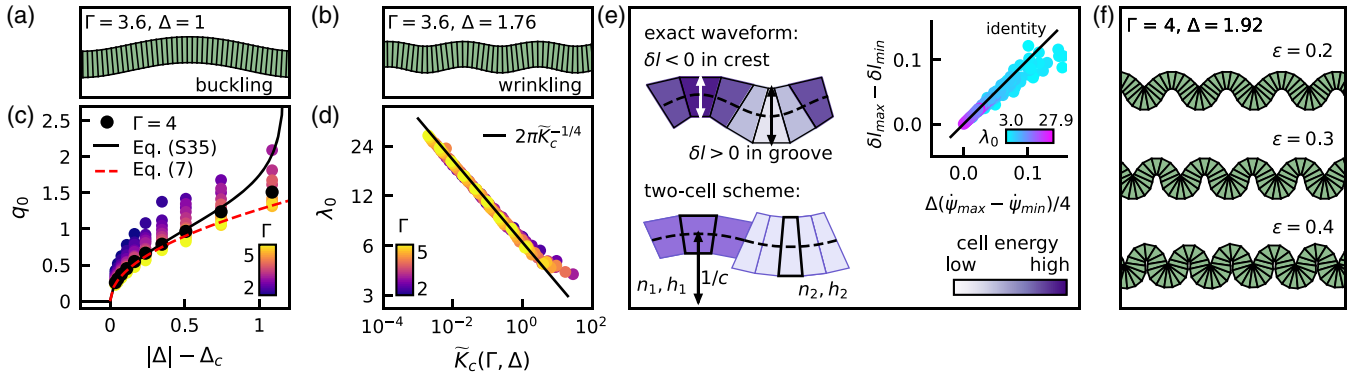

FIG. 3. (a),(b) Buckled and wrinkled shapes at $\Delta = 1$ (a) and $\Delta = 1.76$ (b); $\Gamma = 3.6$ in both cases. (c) Numerically obtained equilibrium wave number q_0 vs $|\Delta| - \Delta_c$. Solid and dashed lines show the exact result [Eq. (S35)] and the result for small $|\Delta| - \Delta_c$ [Eq. (7)], respectively. (d) Equilibrium wavelength λ_0 vs critical phantom-substrate stiffness $\tilde{K}_c$ given by Eq. (S33). (e) Cell-height modulation in a tissue with $\Delta > \Delta_c$ (top) and two-cell scheme (bottom). Inset: cell-height modulation vs curvature modulation; solid line is identity predicted by Ref. [22]. Data points deviate from the identity at small λ_0, where the discrete nature of tissue becomes more pronounced. (f) Compressed tissues for large strains $\epsilon = 0.2$, 0.3, and 0.4.

to the local curvature $\dot{\psi}(\sigma)$: $\delta l(\sigma) \approx \Delta\dot{\psi}(\sigma)/4$ [Fig. 3(e) and Ref. [22]]. Since cells are incompressible, this modulation implies symmetry breaking between the number density of cells in groove (where $\dot{\psi} > 0$) and that in the crest (where $\dot{\psi} < 0$), such that the energetically favorable cells in the segment with the preferred local curvature are packed more densely than elsewhere. For instance, for $\Delta > 0$ the low-energy cells in the groove are taller and narrower than the high-energy cells in the crest [Fig. 3(e)]. We note that in our model, the phase of cell-height modulation depends on the sign of Δ and is not universal like in a wrinkled supported solid plate where the grooves are always thinner than the crests [23] and in a fluidlike film anchored to a solid substrate by a fibrous scaffold where it is the opposite [24].

In our model, cell-height modulation is an emergent phenomenon that occurs even though the properties of the cells are homogeneous across the epithelium. This implies that the wrinkling instability cannot be predicted from the behavior of individual cells whose preferred shape is a trapezoid with height $h_0 = \Gamma^{1/2}$ and curvature $c_0 \approx -2\Gamma^{1/2}\Delta$ [18]. In line with the Gauss-Bonnet theorem, a sheet described by an in-plane periodic curve that carries a bending energy $dw_b/ds = k(c - c_0)^2/2$ favors a flat configuration despite the spontaneous curvature c_0.

To explain the loss of stability in a flat tissue as simply as possible, we consider a waveform consisting of two circular arcs of curvatures $-c$ and $+c$ (i.e., groove and the crest, respectively) subtending an angle ϕ [Fig. 3(e)]. All groove cells are identical and so are those in the crest; we denote the two cell types by indices 1 and 2. The total energy of the waveform is a weighted sum of single-cell energies w_1 and w_2: $W = N(h_1w_1 + h_2w_2)/(h_1 + h_2)$ (Supplemental Material, Sec. VI [20]). In agreement with our elasticity theory, the energy is minimized when groove and crest cells assume different heights ($h_1 \neq h_2$), thereby breaking the groove-crest symmetry. The height difference agrees with the magnitude of cell-height modulation from the elasticity theory: $h_1 - h_2 = c\Delta/2$. Furthermore, this minimal scheme gives the exact critical point $|\Delta| = \sqrt{2}$, where the difference of the energies of the model waveform and the flat tissue $\delta W = N(2 - \Delta^2)c^2/(16\Gamma^{1/2})$ changes sign. In all, this calculation demonstrates that the emergent groove-crest asymmetry in cell height is the dominant mechanism of the wrinkling instability. Previous theories of epithelial elasticity captured this effect to a certain extent, but they did not manage to reproduce the instability due to geometric oversimplifications [17,25].

To check whether the exact mapping of epithelial elasticity to the plate-substrate system [Eq. (5)] also holds for large deformations, we investigate tissue shapes at large strains; we note that the vertex model includes the nonlinear mechanics absent in our harmonic theory. Unlike thin plates that undergo period bifurcations and wrinkle-to-fold transition when supported by solid and liquid substrates, respectively [4,5,7], we find that epithelia remain wrinkled with a single mode even at large deformations [Fig. 3(f)]. The absence of the wrinkle-to-fold transition, which appears in thin plates attached to fluid substrates, can be intuitively understood from the point of view of cell-height modulation. The groove-crest asymmetry allows the tissue side subjected to a higher surface tension to decrease its area compared to the opposite, less tense, side. Compared to the wrinkled configuration, this effect would be much less pronounced in a fold configuration, where most of the tissue would be flat with cells having apical and basal sides of equal size.

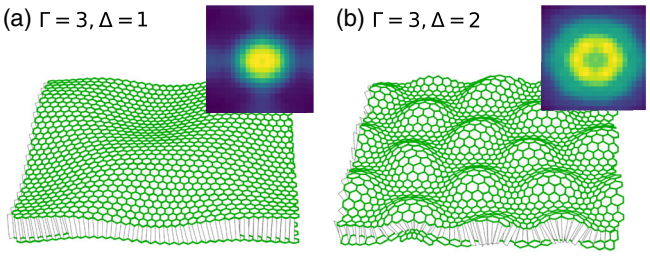

FIG. 4. Epithelial sheets at $\Gamma = 3$ for $\Delta = 1$ (a) and $\Delta = 2$ (b) at isotropic in-plane strain of $\epsilon = 0.02$. Insets show Fourier transforms of the apical surfaces, averaged over 100 instances obtained from randomly perturbed flat initial configurations.

3D model.—Our reduced-dimensionality model considers the cross section of the tissue along the waveform, effectively assuming a fixed cell dimension in the perpendicular direction. To show that the buckling-to-wrinkling transition is not an artifact of this assumption, we employ a 3D vertex model [26] where the epithelium is represented by a sheetlike packing of six coordinated polyhedral cells—and we observe buckled states at small Δ and wrinkled states at large Δ in agreement with the 2D model. This is illustrated in Figs. 4(a) and 4(b), which show that depending on Δ, a small isotropic in-plane compression results either in a buckled state characterized by a wave number defined by patch size D [Fig. 4(a)] or in a wrinkled state with a well-defined q larger than $2\pi/D$ [Fig. 4(b)]. A detailed analysis of the transition including the evaluation of the critical differential surface tension carried out in a model that permits topological changes is beyond the scope of this work and is relegated to a forthcoming publication.

Discussion.—Our elasticity theory of unsupported epithelial monolayers demonstrates that intraepithelial tensions drive the formation of wrinkles similar to those observed in thin plates supported by thick substrates even though the underlying physics relies solely on surface mechanics and includes no bulk deformations. These results are important because they show that a sheetlike biological tissue can wrinkle even when its mechanical interaction with the environment is weak, say, because the adjacent substances are gel-like and cannot sustain long-term shear stresses. Our model suggests that these effectively unsupported epithelial tissues, which appear, e.g., in some early embryos [27] and in various tissue-derived

epithelial organoids [28–33], can autonomously control their surface patterns just as if they rested on a substrate.

At the cell scale, epithelial wrinkling is based on the breaking of the groove-crest symmetry due to cell-height modulation along the waveform [Fig. 3(e)], which was observed in cell monolayers cultured on wavy substrates [34,35] and described using the same microscopic cell-level framework as employed here [Eq. (2)].

According to our results, the wrinkling wavelength can range between less than ∼10 and ∼100 cell sizes when the apico-basal differential tension $|\Gamma_a - \Gamma_b|$ is comparable to the lateral tension Γ_l [Fig. 3(c)]. Given that the surface tensions are often of similar magnitude as shown, e.g., in Ref. [13], our proposed wrinkling mechanism can be readily studied either *in vitro* or *in vivo*—say, using optogenetic tools or genetic manipulations [36] and possibly employing explants [10]—so as to verify its postulated role in embryonic and organoid morphogenesis. If confirmed, our mechanism would complement existing theories of tissue wrinkling, including constrained expansion [7–9,37,38], packing of cell nuclei [39], and the buckling-without-bending effect [24].

We thank Eric Wieschaus, Jan Rozman, Simon Godec, Miha Brojan, Jan Zavodnik, Andrej Košmrlj, Edouard Hannezo, and the members of the Theoretical Biophysics Group at Jožef Stefan Institute for fruitful discussions. We acknowledge the financial support from the Slovenian Research Agency (research project No. J1-3009 and research core funding No. P1-0055).

*Corresponding author.
matej.krajnc@ijs.si

[1] Y. Klein, E. Efrati, and E. Sharon, Science **315**, 1116 (2007).
[2] E. Efrati, E. Sharon, and R. Kupferman, J. Mech. Phys. Solids **57**, 762 (2009).
[3] E. Cerda and L. Mahadevan, Phys. Rev. Lett. **90**, 074302 (2003).
[4] L. Pocivavsek, R. Dellsy, A. Kern, S. Johnson, B. Lin, K. Y. C. Lee, and E. Cerda, Science **320**, 912 (2008).
[5] F. Brau, H. Vandeparre, A. Sabbah, C. Poulard, A. Boudaoud, and P. Damman, Nat. Phys. **7**, 56 (2011).
[6] O. Oshri, F. Brau, and H. Diamant, Phys. Rev. E **91**, 052408 (2015).
[7] F. Brau, P. Damman, H. Diamant, and T. A. Witten, Soft Matter **9**, 8177 (2013).
[8] E. Hannezo, J. Prost, and J.-F. Joanny, Phys. Rev. Lett. **107**, 078104 (2011).
[9] A. E. Shyer, T. Tallinen, N. L. Nerurkar, Z. Wei, E. S. Gil, D. L. Kaplan, C. J. Tabin, and L. Mahadevan, Science **342**, 212 (2013).
[10] O. Luu, R. David, H. Ninomiya, and R. Winklbauer, Proc. Natl. Acad. Sci. U.S.A. **108**, 4000 (2011).
[11] T. P. J. Wyatt, J. Fouchard, A. Lisica, N. Khalilgharibi, B. Baum, P. Recho, A. J. Kabla, and G. T. Charras, Nat. Mater. **19**, 109 (2020).
[12] J. Fouchard, T. P. J. Wyatt, A. Proag, A. Lisica, N. Khalilgharibi, P. Recho, M. Suzanne, A. Kabla, and G. Charras, Proc. Natl. Acad. Sci. U.S.A. **17**, 117 (2020).
[13] L. Sui, S. Alt, M. Weigert, N. Dye, S. Eaton, F. Jug, E. W. Myers, F. Jülicher, G. Salbreux, and C. Dahmann, Nat. Commun. **9**, 4620 (2018).
[14] M. Gracia, S. Theis, A. Proag, G. Gay, C. Benassayag, and M. Suzanne, Nat. Commun. **10**, 2951 (2019).
[15] J. Rozman, M. Krajnc, and P. Ziherl, Nat. Commun. **11**, 3805 (2020).
[16] M. Krajnc, N. Štorgel, A. Hočevar Brezavšček, and P. Ziherl, Soft Matter **9**, 8368 (2013).
[17] M. Krajnc and P. Ziherl, Phys. Rev. E **92**, 052713 (2015).
[18] N. Štorgel, M. Krajnc, P. Mrak, J. Štrus, and P. Ziherl, Biophys. J. **110**, 269 (2016).
[19] J. Derganc, S. Svetina, and B. Žekš, J. Theor. Biol. **260**, 333 (2009).
[20] See Supplemental Material at http://link.aps.org/supplemental/10.1103/PhysRevLett.130.198401 includes the derivation of the elasticity theory and a description of the vertex model.
[21] Equation (7) in Ref. [7], $By^{(4)} + F\ddot{y} + Ky = 0$, is a general force-balance equation for a thin plate resting on a bulk substrate. By inserting the ansatz $y(s) = y_0 \sin(qs)$, one obtains an algebraic equation for the wave number, which reads $Bq^4 + Fq^2 + K = 0$, where K is the substrate's stiffness. In case of a liquid substrate, $K = \rho g$ is an effective stiffness due to fluid's weight; here ρ and g are the fluid's mass density and gravitational acceleration, respectively.
[22] Relation $\delta l(\sigma) - \delta l_0 \approx \Delta\dot{\psi}(\sigma)/4$ follows from Eq. (S20) in Supplemental Material when second derivatives as well as μ are neglected.
[23] M. Holland, S. Budday, A. Goriely, and E. Kuhl, Phys. Rev. Lett. **121**, 228002 (2018).
[24] T. A. Engstrom, T. Zhang, A. K. Lawton, A. L. Joyner, and J. M. Schwarz, Phys. Rev. X **8**, 041053 (2018).
[25] P. A. Haas and R. E. Goldstein, Phys. Rev. E **99**, 022411 (2019).
[26] J. Rozman, M. Krajnc, and P. Ziherl, Eur. Phys. J. E **44**, 99 (2021).
[27] L. Wolpert, C. Tickle, A. Martinez Arias, P. Lawrence, and J. Locke, *Principles of Development*, 6th ed. (Oxford University Press, Oxford, 2019).
[28] T. Sato, R. G. Vries, H. J. Snippert, M. van de Wetering, N. Barker, D. E. Stange, J. H. van Es, A. Abo, P. Kujala, P. J. Peters, and H. Clevers, Nature (London) **459**, 262 (2009).
[29] T. Zietek, E. Rath, D. Haller, and H. Daniel, Sci. Rep. **5**, 16831 (2015).
[30] P. Jung, T. Sato, A. Merlos-Suárez, F. M. Barriga, M. Iglesias, D. Rossell, H. Auer, M. Gallardo, M. A. Blasco, E. Sancho, H. Clevers, and E. Batlle, Nat. Med. **17**, 1225 (2011).
[31] M. Huch, C. Dorrell, S. F. Boj, J. H. van Es, V. S. W. Li, M. van de Wetering, T. Sato, K. Hamer, N. Sasaki, M. J. Finegold, A. Haft, R. G. Vries, M. Grompe, and H. Clevers, Nature (London) **494**, 247 (2013).

[32] N. Barker, M. Huch, P. Kujala, M. van de Wetering, H. J. Snippert, J. H. van Es, T. Sato, D. E. Stange, H. Begthel, M. van den Born, E. Danenberg, S. van den Brink, J. Korving, A. Abo, P. J. Peters, N. Wright, R. Poulsom, and H. Clevers, Cell Stem Cell **6**, 25 (2010).

[33] C. Greggio, F. De Franceschi, M. Figueiredo-Larsen, S. Gobaa, A. Ranga, H. Semb, M. Lutolf, and A. Grapin-Botton, Development (Cambridge, U.K.) **140**, 4452 (2013).

[34] M. Luciano, S.-L. Xue, W. H. De Vos, L. Redondo-Morata, M. Surin, F. Lafont, E. Hannezo, and S. Gabriele, Nat. Phys. **17**, 1382 (2021).

[35] N. Harmand, J. Dervaux, C. Poulard, and S. Henon, Eur. Phys. J. E **45**, 53 (2022).

[36] G. Martínez-Ara, N. Taberner, M. Takayama, E. Sandaltzopoulou, C. E. Villava, M. Bosch-Padrós, N. Takata, X. Trepat, M. Eiraku, and M. Ebisuya, Nat. Commun. **13**, 5400 (2022).

[37] V. Balbi, M. Destrade, and A. Goriely, Phys. Rev. E **101**, 022403 (2020).

[38] T. Tallinen, J. Y. Chung, F. Rousseau, N. Girard, J. Lefèvre, and L. Mahadevan, Nat. Phys. **12**, 588 (2016).

[39] E. Karzbrun, A. Kshirsagar, S. R. Cohen, J. H. Hanna, and O. Reiner, Nat. Phys. **14**, 515 (2018).